Petroleum and Coal

Article **Open Access**

CHARACTERIZATION OF PORE SYSTEMS IN CARBONATE USING 3D X –RAY COMPUTED TOMOGRAPHY

Spariharijaona Andriamihaja*[1], E. Padmanabhan[1] and Joel Ben –Awuah[2]

[1] *Department of Geosciences, Faculty of Petroleum Engineering and Geoscience, Universiti Teknologi PETRONAS , Seri Iskandar 32610, Malaysia*
[2] *Department of Petroleum Engineering, Faculty of Engineering, Technology and Built Environment, UCSI University, Jalan Choo Lip Kung, Taman Taynton View, 5600 Cheras, Kuala Lumpur, Malaysia*

Received June 11, 2016; Accepted September 20, 2016

Abstract

It is well-known that prediction of petrophysical parameters which is closely linked to pore system complexities is always challenging especially for carbonate rock study. This paper describes and characterizes the pore systems within a carbonate rock, using X- Ray computed tomography imaging. After processing and analyzing series of digital thin sections, pore space is differentiated from matrix and eventually from grains. Pore space parameters such as pore type, connectivity, size, and porosity were extracted and described. The analysis of pore connectivity is more reliable in 3D. The pore type evaluation in 2D points out that the observed pores are moldic, separate – vug while in 3D, some are solution - enlarged as touching –vug pores. The sample is dominated by touching – vug pores by taking into account the pore volume and the connectivity analysis in 3D view. The pore shapes appear irregular and are developed randomly. The shape of the pore varies significantly between intervals of 440µm. The pore size variation differs between each pore. The use of 3D pore model analysis is carried out to complement routine petrographic technique is complementary in order to enhance the classification and the characterization of pore systems in carbonate.

Keywords: carbonate rock; pore connectivity; pore size; pore shape; 3D.

1. Introduction

Storage capacity of reservoir (porosity) and ability of hydrocarbon flowing within and out of the reservoir (permeability) are greatly influenced by pore attributes such as pore types, geometry, connectivity, size, and distribution [1]. In carbonate rocks, these pore attributes are very complex due to carbonate fabric heterogeneities, results of depositional environment and diagenetic processes [2-3]. Several researches have been conducted to elucidate these complexities, in order to have a better understanding of geological and petrophysical parameters controlling the fluid flow of the carbonate reservoir [4-7]. In pore characterization study of carbonate, focus are mainly on pore type identification derived essentially from routine thin sections, or digital images [8-9]. The quantitative attributes such as pore size distribution and porosity are usually derived from other techniques such as Mercury Injection method, or Nuclear Magnetic Resonance (NMR) [10-11].

The introduction of X – ray Computed Tomography images (CT scan) as a geoscience tool helps to understand in detail the internal structure of reservoir rocks [12-13]. This technique is mainly used in the reservoir properties prediction [14-15] and rock physic studies [16-17].

Even though the complexities of the pore system within carbonate reservoir rock have been extensively studied in 2D using thin sections and Scanning Electron Microscopy (SEM), determination of pore system in carbonate rock remains a challenge. Therefore, the objective of this paper is to determine the different pore attributes (pore type, pore size, geometry, connectivity and distribution) by 3-D pore network system within carbonate rocks.

2. Materials and methods

Carbonate rock sample from onshore Sarawak Basin, Malaysia is studied in this paper. Optical thin section and SEM (Scanning Electron Microscopy) images are used to characterize and describe the different components and structures within the carbonate rock in order to highlight the advantages and the limitations of these techniques. A core plug of 1 inch diameter is scanned, using InspeXio Microfocus CT system 255 located in Universiti Teknologi PETRONAS. As the quality of the output images is function of the ability of the sample to attenuate the X-ray, and after several tests, the optimal X-ray parameters are set as 70 µÅ for the intensity and 190KV for the tube voltage. The output data image is composed by 677 slices with resolution of 36 µm. The attenuation rate of X-rays within each pixel of image is represented by gray scale color varying from 0 - 255. The 0 and 255 values correspond to black and white respectively. Therefore, the cut off value of two phases (void and material phases) is 69. The lower band width value in gray scale corresponds to void phase and the remaining band width is associated to material phase (grains and cement).

3. Results and discussion

Macroscopic description

The sample is highly consolidated and dominated by lime mud (micrite). The color of the sample varies from grayish yellow to moderate yellowish brown. Intercalation of slightly wavy less porous (50%) and more porous (50%) laminae provides an indication that sample could have a possibly complicated porosity pattern (Figure 1). These laminations have thicknesses that range from 0.5cm to 1 cm indicating a non-consistency of thickness. This suggests inconsistency in the precipitation events. The boundary between the porous and non-porous laminae may occasionally be occupied by platy-shaped pores which are termed as interlaminae pores (Figure 1). These pores may have developed as a result of pressure release in the rock system that created fissures along planes of weaknesses. These pores tend to have calcitic infilling thereby reducing the porosity in most places. These pores are extremely limited in their lateral continuity, tortuosity and interconnectivity. The development of these pores with depth remains unclear. The observed pores at macroscale are not connected and larger than the average grain size. Therefore, the majority of pore systems are classified as moldic separate – vug pore [18] (Figure 1). The sample is classified as mudstone using Dunham's classification [19].

Figure 1. Hand specimen lime-mud showing intercalation of less porous and more porous structureless laminae. The pores show different shapes (platy to spheric) and size (millimeter to centimeter).

Microscopic description

The mudstone shows a structureless lamination intercalated between two micro wavy laminae, with a thickness less than 100 μm (Figure 2a). The pores only occur in these structureless mud laminae. The pores contain late phase crystallized calcite grains. The cements are also developed as granular calcitic cements within the pore throats leading to the formation of isolated pores. Therefore, the isolated pores are not entirely characteristic of the primary depositional environment. The connectivity analysis in thin section is only limited between two different pores occuring in the same plane. The diameters of these pores vary from 100 μm to 4000 μm. The shapes of the pores are angular to subangular, controlled by the new calcitic cement. The sphericity of the pores varies from 0.5 to 0.9. Other spaces occur between the newly formed crystals, and are classified as intercrystalline pores (Figure 2b). The size of the pores are less than 100 μm.

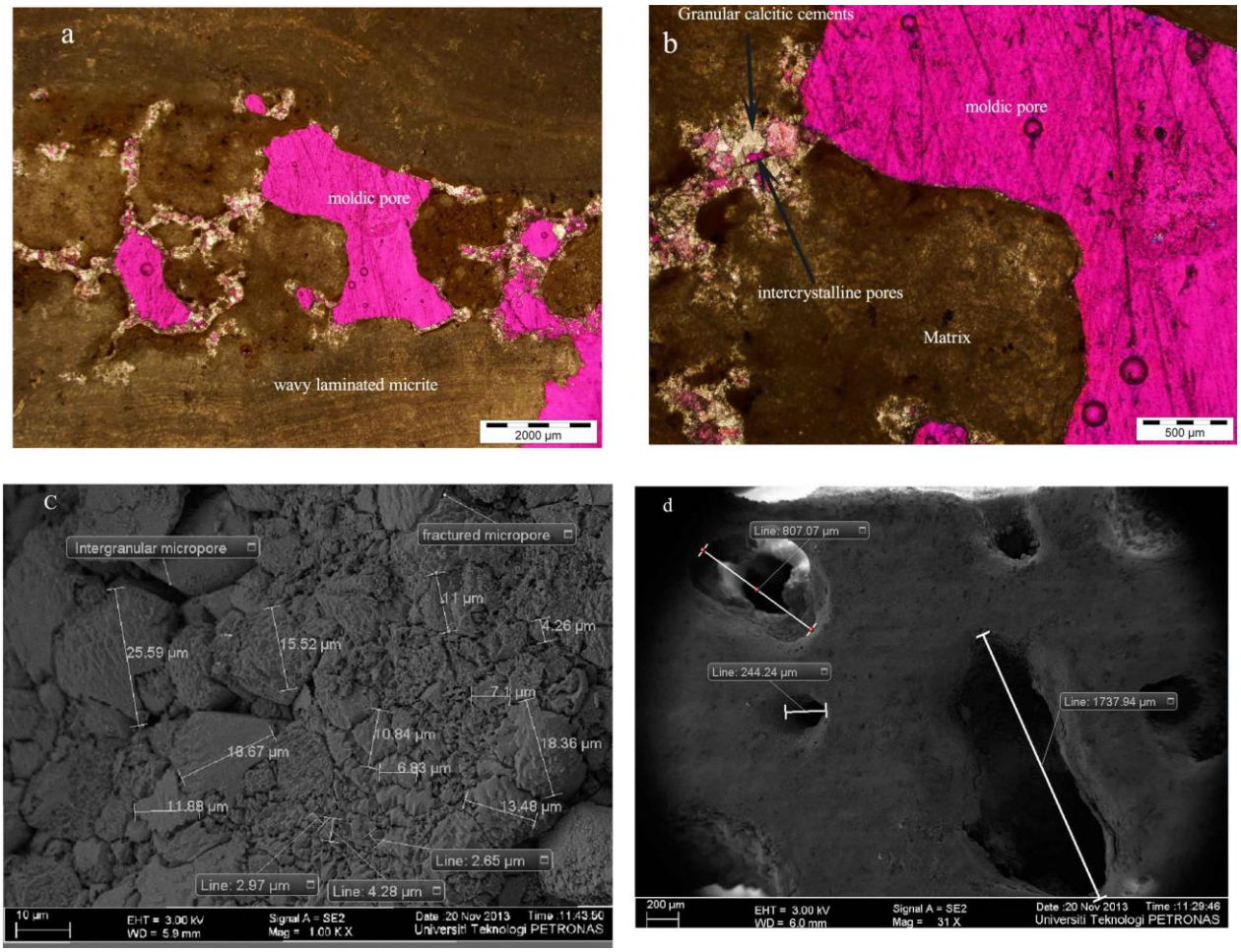

Figure 2. a-Cross- polarized thin section a- showing two wavy laminated micrite layers intercalated by very porous layer and where the pores are moldic separate vug pores (pink). b-The pore throats plugged by newly granular calcitic cements, and the presence of intercrystalline pores c- SEM of calcite minerals showing variation in grain size, shapes. The pores are intergranular and fractured pores. d- SEM at surface of the sample, showing unconnected pores, with different shapes and sizes.

The carbonate sample is a result of several diagenetic processes after deposition. This sample is most likely affected by dissolution process creating the pore. The cement type indicates that cementation occurred in meteoric – vadose and burial environments. Therefore, the diagenetic processes lead to variation of pore size, shape and connectivity. These variations influence the quality of the reservoir rock and the volume of hydrocarbon that can be stored in the rocks. The

variation in pore connectivity will influence the permeability and flow properties of the rock. The pores observed in thin section are isolated and classified as moldic separate – vug pores, which are in good agreement with the pore analysis at macroscale.

Scanning Electron Microscope

The grains are angular to subangular with sphericity ranging from 0.7 to 0.9 [20]. The diameters of these grains vary from 2.65μm to 25.59μm. The observed micropore systems are intergranular and fractured pores (Figure 2c).

At the surface of the sample, the pores are unconnected. They vary in shapes (elongated, slightly rounded), and in diameters (from164.34 μm to1434.18 μm) (Figure 2d). However, the SEM image analysis is only limited at certain depth, ignoring the internal development of pores within the rock.

Computed Tomography Image Analysis

- *Classification and connectivity in 2D*

The qualitative analysis of each slice within 3 arbitrary planes (XY; XZ; YZ) shows that most of the individual pores are very large , isolated and surrounded by the matrix fabric (Figure 3a). Furthermore, the individual grains are undetectable as they are very small (smaller than the voxel size). Therefore, the mud supporting the fabric (matrix) and the grains are undifferentiated (Figure 3b). At the scale of study, these pores are mainly classified as moldic, separate – vug pores in mud – dominated fabric.

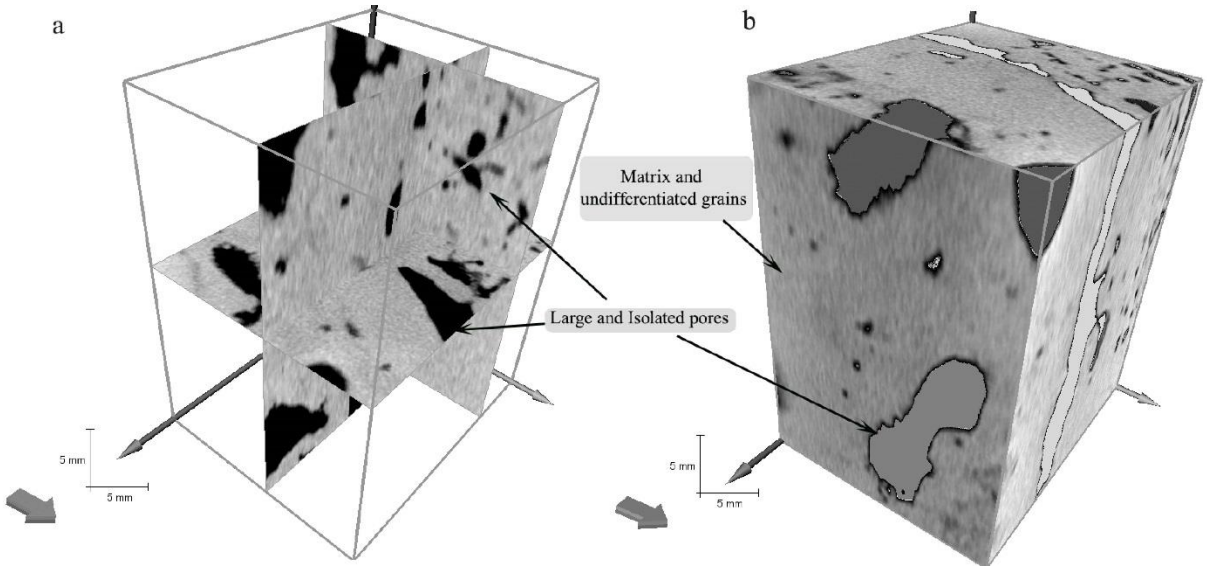

Figure 3. a- Three slices within the three arbitrary planes, showing very large and isolated pores. b- 3D CT scan images where the grains and the matrix are undifferentiated

The pore system is composed by [20]:

- Interconnected channels (connectivity) represented by connection of one or several segments (figure 4a,b,c,d,e,f) and
- Pores composed by groups of radial lines.

Within the same arbitrary plane such as in XY plane (Figure 4a and Figure 4b) or XZ plane (Figure 4c and figure 4d) or in YZ plane (Figure 4e and figure 4f), the pore connectivity varies from slice to another. However, each slice contains both connected pores represented by inter-connected channels and isolated pores, and shows variation in distribution. Therefore, this implies that the pore connectivity studied in 2D is not well expressed.

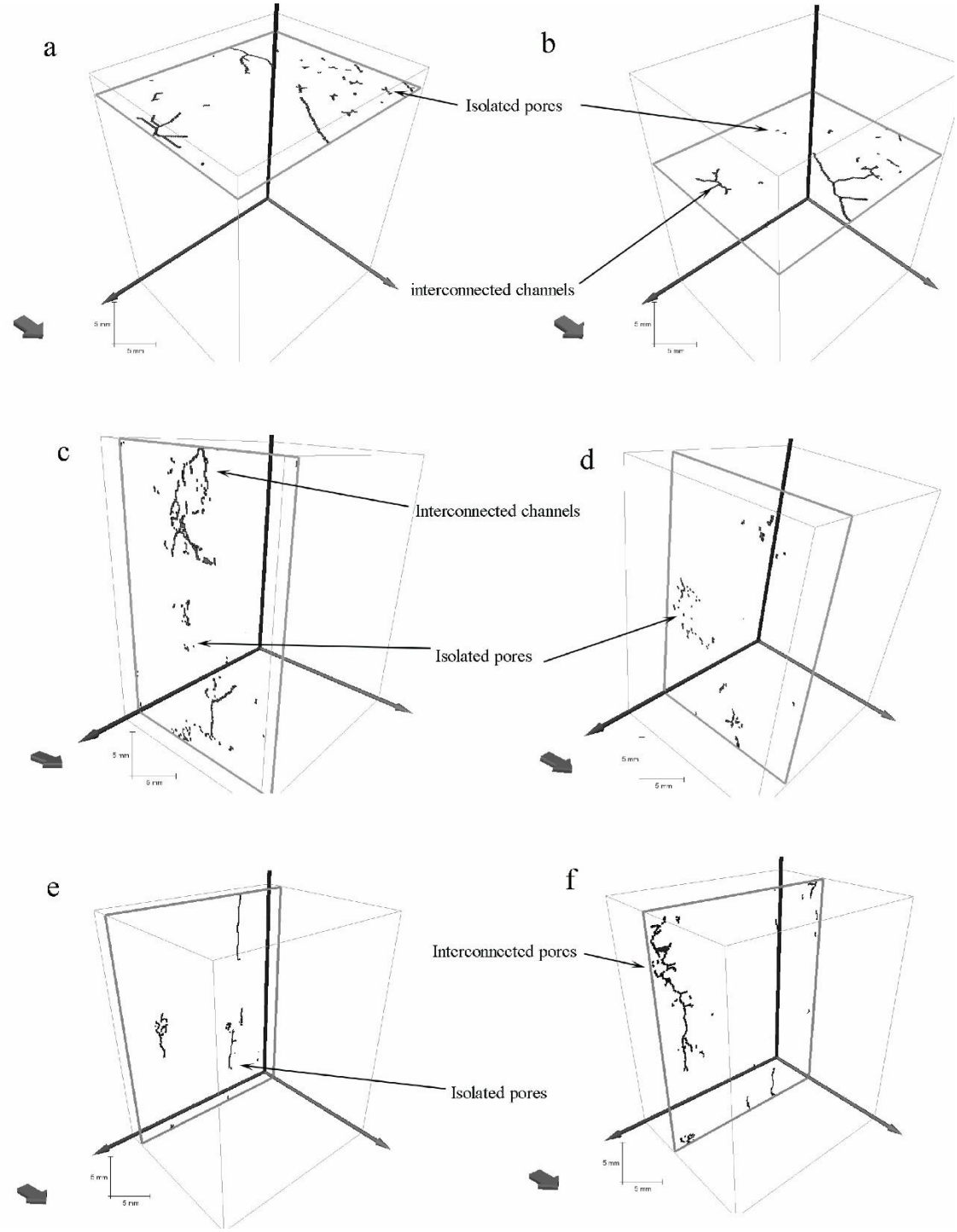

Figure 4. Pore connectivity variation in 2D displaying interconnected channels and isolated pores. a- within XY plane at slice 184, b- within XY plane at slice 261,c - within XZ plane at slice 25, d-within XZ plane at slice 71,e - within YZ plane at slice 178, f - within YZ plane at slice 211

- *Pore classification and connectivity in 3D*

In 3D view, connected pore systems are represented by line (throat), composed by series of segments and nodes (more than two segments). On the other hand, isolated pores are represented by only one segment and ended by two nodes at the extremity. Therefore, the 3D pore

network model reveals that many pores are actually connected within all of the three directions. Some pores that are initially classified as isolated pores in 2D view are actually connected with other pores occurring in the third plane. Therefore, in 3D, the differentiation between separate and touching vug pores should be based on 3D connectivity of the pore system (Figure 5a) as opposed to 2D assessment.

Among the 253 individual pores which are identified, 47 pores are connected and classified as solution - enlarged, touching – vug pore. The total length of the connected pores within the sample is 692.94mm, and the length of each connected pore varies from 231.41 to 2.81mm. The total volume of 253 pores is 561.04 mm^3. 98.21% of this total volume corresponds to 47 connected pores. On the other hand, 206 individual pores representing 1.79% of the total pore volume are isolated and classified as moldic separate – vug pores.

Therefore, integrating the pore connectivity from 3D pore network model in pore classification, two pore types are identified solution - enlarged touching – vug and moldic separate – vug pores (Figure 5b). By taking into account the pore volume, the sample is actually dominated by the solution - enlarged, touching – vug pore.

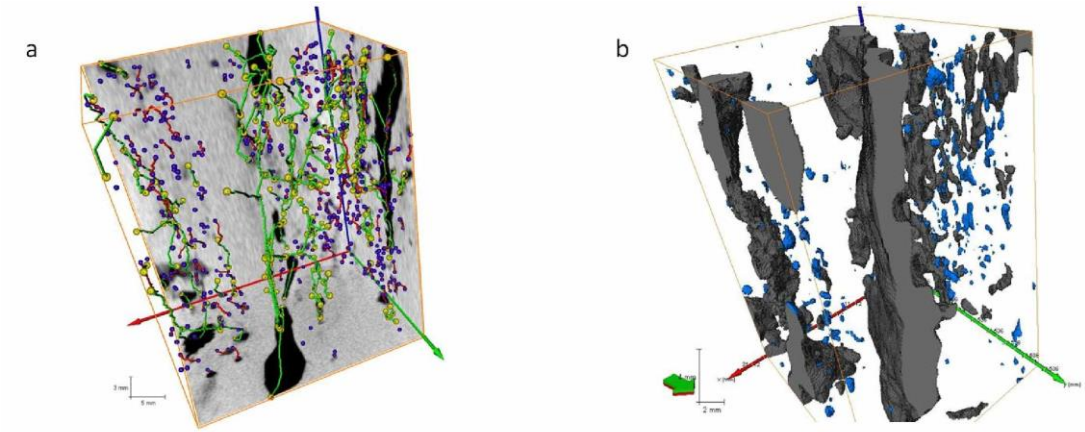

Figure 5. a-3D pore connectivity model where the green tubes with yellow nodes are connected pores and red tubes with blue nodes are isolated pores; b-3D pore model where the gray pores represent solution - enlarged, pores, grouped in touching – vug pores while the blue pores are moldic separate – vug pores

- *Pore Size Analysis*

253 identified pores show different size within the core plug. Pore volume varies from 561.04 mm^3 to 0.01 mm^3 with a mean volume of 24.58mm^3. In order to determine the pore size variation within the slices, 6 representative pores (Figure 6) were selected randomly and the surface areas of each pore per slice in the arbitrary XY plane were measured and analyzed.

Within the range of studied slices, pore 1 (Figure 7a) starts and ends as an opened pore with a general decreasing of pore size. Compared to the other pores, pore 1 has the largest size. On the other hand, the pore 2 (Figure 7b) starts as closed system and reaches the maximum size at slice 100.The size of pore 2 remains approximately 5mm^2 from slice 0 to 75 and then increases exponentially until slice 100, reaching 17.82 mm^2.

The pore size of pore 3 (Figure 7c) decreases gradually and then after, increases exponenttially reaching the peak of 55.99 mm^2 in the slice 31. From this peak, the pore size of pore 3 decreases gradually, but remains still opened system within the slice100.

Pore 4 (Figure 7d), 5 (Figure 7e) and 6 (Figure 7f) is closed system pore as within the study slices, the pore sizes start and end at the minimum size. However, their graphs show that there are 3 phases of pore size development. The first phase corresponds to the development of pores itself, where the pore size increases from 0 mm^2 to a certain maximum pore size. The second phase is where the pore reachs its highest size and remains more or less constant

throught several slices. The third phase corresponds to a phase where the pore size starts to decline until minimum size.

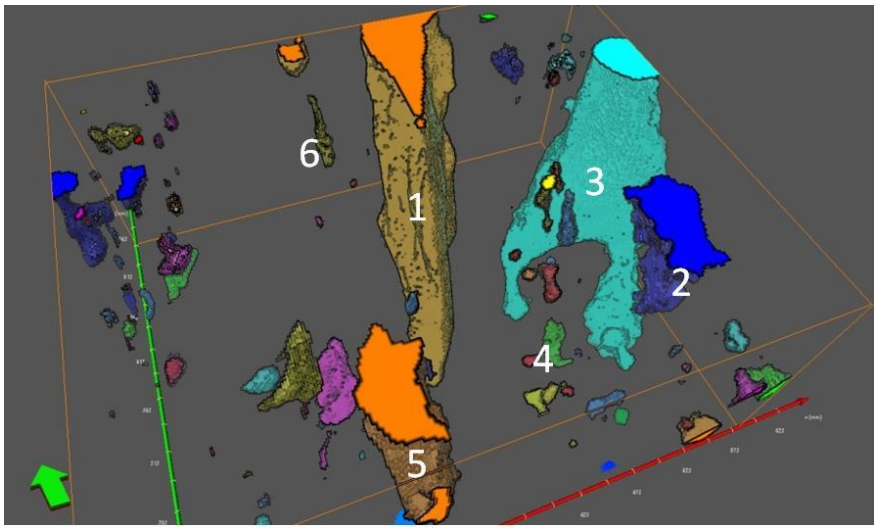

Figure 6. Six selected pores for pore size analysis

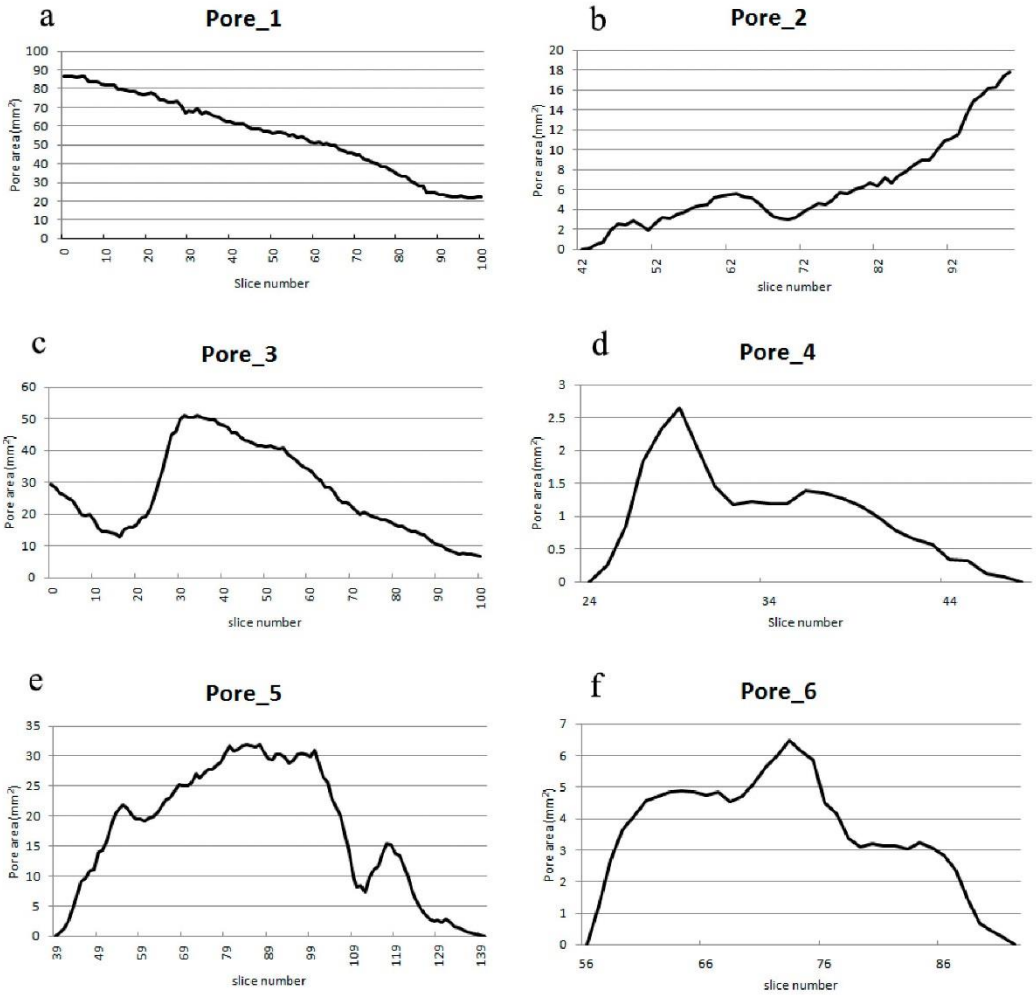

Figure 7. Pore size distribution along Z- axis: a- pore 1; b-pore 2; c- pore 3; d-pore 4; e- pore 5; f-pore 6

- *Porosity distribution*

In order to evaluate the porosity of the entire core plug, statistical analysis was carried out. Therefore, within the studied sample, the porosity varies between 6.41% and 13.05%, with an average of 9.51%. The porosity distribution is normal distribution with a positive skewness of 0.26 and kurtosis of -0.726. This distribution indicates heterogeneity of porosity within a sample at millimeter to centimeter scale.

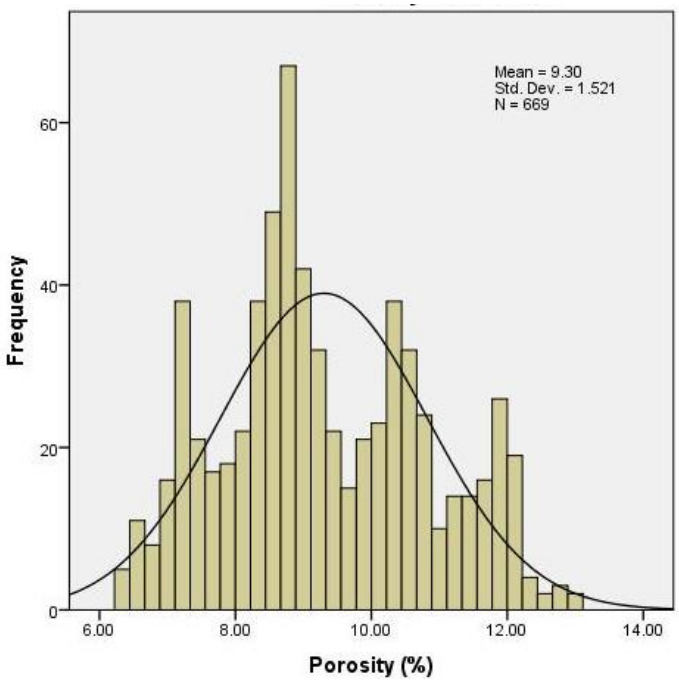

Figure 8. Porosity distribution showing normal distribution with an average porosity of 9.51%

By considering slices (slice 2 and 141), with a same given porosity (11.20%), the pore systems show different spatial distribution, shape (Figure 9a and b). However, each pore has different size but the total pore surface for both slices is identical.

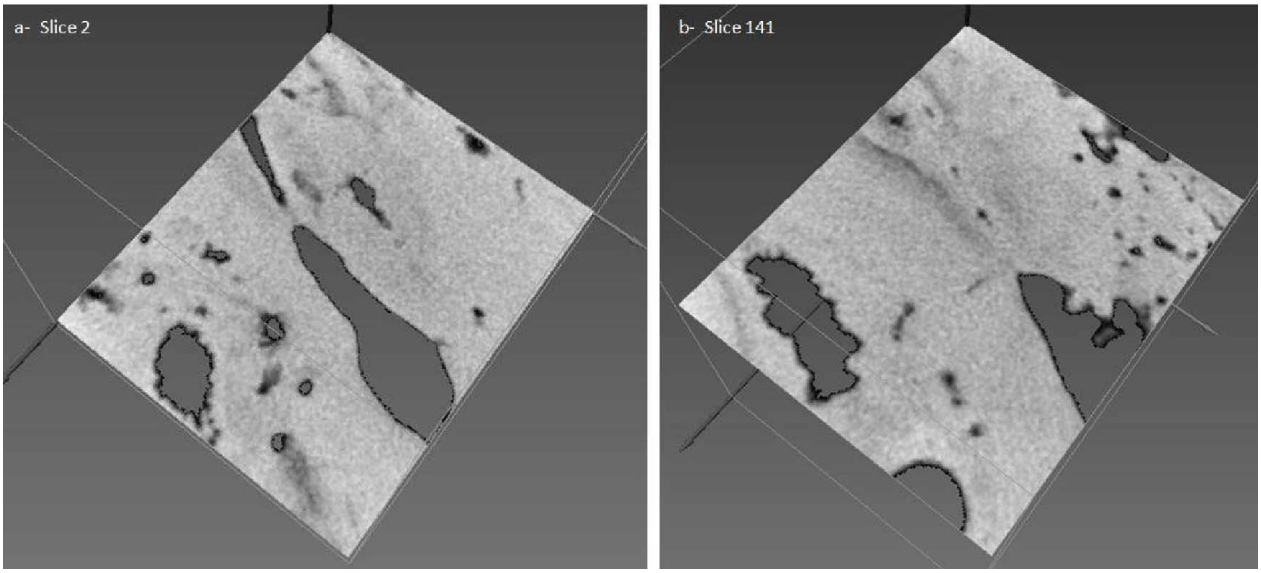

Figure 9. Two different slices with the same porosity (11.2%) but displaying different spatial distribution and shape a- slice 2; b- slice 141

4. Conclusion

3D pore network modeling and analysis of digital thin sections derived from computed tomography image have been used to characterize and evaluate the pore systems within a carbonate rock plug. The analysis of digital thin sections and connectivity show that in 2D plane, pores appear to be isolated and classified as moldic separate – vug pore in mud – dominated fabric. However, when all these digital thin sections are integrated together, it becomes evident that most of the pores are actually connected in 3D view. The connected pores dominate the total pore volume, and corresponds to 98.21%. Integrating 3D pore connectivity in pore classification, the connected pores in the sample can therefore be reclassified as solution - enlarged, touching – vug pores.

It is observed that the vuggy pore size development shows three phases which are the pore enlargement phase followed by pore stagnation phase and pore reduction phase.

The analysis of each slice which can be assimilated to a routine optical thin section points out that the porosity values vary significantly from one slice to another. In this point of view, it is difficult to appreciate the representative porosity with only one value derived from thin section. Therefore, a statistical approach is proposed to derive porosity from CT scan imaging which is more reliable as large amount of data is analyzed.

The variations of pore shape, size and porosity between each slice imply that the conditions for the development of each pore at micro scale are different. Therefore, the introduction of 3D pore network model derived from CT scan image improves pore classification and characterization of carbonate.

The 3D modeling of CT scan image analysis contributes to the accuracy of pore characterization output. The method enhances carbonate characterization and provides more information on the pore systems within the sample. The uses of this method in combination with routine petrographic technique will enhance the classification and the characterization pore systems in carbonate.

Acknowledgment

This study is supported by YUTP grant awarded to Dr. Eswaran. Padmanabhan.

References

[1] Ehrilich R, Davies D. Image Analysis Of Pore Geometry: Relationship To Reservoir Engineering and Modeling: Spe (Society Of Petroleum Engineers) 1989.

[2] Flugel E. Microfacies Of Carbonate Rocks: Analysis, Interpretation and Application: Springer Berlin Heidelberg, 20041- 996 P.

[3] Dravis JJ. Carbonate Applied To Hydrocarbon Exploration And Exploitation, 2007.

[4] Archie G. Classification of Carbonate Reservoir Rocks and Petrophysical Considerations: Aapg Bulletin, 1952; 36(2):278–298, DOI:10.1306/3d9343f7-16b1-11d7-8645000102c1865d.

[5] Choquette PW, Pray LC. Geologic Nomenclature and Classification of Porosity In Sedimentary Carbonates: Aapg Bulletin, 1970; 54(2): 207–250.

[6] Lucia FJ. Rock-Fabric/Petrophysical Classification Of Carbonate Pore Space For Reservoir Characterization: Aapg Bulletin, 1995; 79(9): 1275–1300, DOI:10.1306/7834d4a4-1721-11d7-8645000102c1865d.

[7] Lønøy A., Making Sense of Carbonate Pore Systems: Aapg Bulletin, 2006; 90, (9): 1381–1405, DOI:10.1306/03130605104.

[8] Ruzyla, K. 1986, Characterization of Pore Space by Quantitative Image Analysis: Spe Formation Evaluation, No. August, P. 389–398.

[9] Anselmetti FS, Luthi S, Eberli GP. Quantitative Characterization of Carbonate Pore Systems by Digital Image Analysis 1. 1998; 10(10): 1815–1836.

[10] Mai A, Kantzas A. Porosity Distribution of Carbonate Reservoirs Using Low Field Nmr: Petroleum Society of Canada. 2002.

[11] Abojafer SM. The Use Of High Pressure Micp Data In Reservoir Characterization, Developing A New Model For Libyan Reservoirs: Society Of Petroleum Engineers. 2009
[12] Mees F, Swennen R, Van Geet M, Jacobs P. Applications of X -Ray Computed Tomography in The Geosciences: Geological Society, 2003, London, Special Publications, No. 215.
[13] Kayser A, Knackstedt MA, Ziauddin M. 2006, A Closer Look At Pore Geometry: Oilfield Review, P. 4–13.
[14] Arns CH, Bauget F, Limaye A, Sakellariou A, Senden T, Sheppard A, Sok RM, Pinczewski V, Bakke S, Berge LI, Oren PE, Knackstedt MA. Pore Scale Characterisation Of Carbonates Using X-Ray Microtomography. Society of Petroleum Engineers 2004, SPE-90368-PA.
[15] Knackstedt MA, Arns CH, Bauget F, Sakellariou A, Senden TJ, Sheppard AP, Sok RM. 2006, Quantitative Transport Properties of Granular Material Calculated From X-Ray μCT Images. JCPDS-International Centre for Diffraction Data 2006 ISSN 1097-0002: 92-97.
[16] Abraham S, Grader AB, Clark S, Al-Dayyani T, Nur A. 2009, Computation of Porosity And Permeability of Sparic Carbonate Using Multi- Scale Ct Image: International Symposium of The Society of Core Analysts, P. 1–12.
[17] Li G, Diaz E, Nur A. 2010, Rock Physical Properties Computed From Digital Core And Cuttings With Applications To Deep Gas Exploration and Development: Proceedings of Spe Deep Gas Conference And Exhibition, DOI:10.2118/131601-Ms.
[18] Lucia FJ. 1983, Petrophysical Parameters Estimated From Visual Descriptions Of Carbonate Rocks : A Field Classification Of Carbonate Pore Space: No. March.
[19] Dunham RJ. 1962, Classification Of Carbonate Rocks According To Depositional Textures: Aapg Memories, P. 108–121.
[20] Krumbein WC., Measurement and geological significance of shape and roudness of sedimentary particles: Journal of Sedimentary Petrology. 1941; 11(2): 64–72.
[21] Youssef S, Rosenberg E, Gland N, Bekri S, Vizika O. 2007, Quantitative 3d Characterisation Of The Pore Space Of Real Rocks : Improved μ -Ct Resolution And Pore Extraction Methodology: International Symposium of the Society of Core Analysts, p. 1–13.

Corresponding author: Sparihariaona Andriamihaja, andriamis@yahoo.f